ACADEMIC PRESS

Available online at www.sciencedirect.com

SCIENCE DIRECT®

Journal of Sound and Vibration 266 (2003) 847–874

JOURNAL OF SOUND AND VIBRATION

www.elsevier.com/locate/jsvi

Optimal control of structures with semiactive-tuned mass dampers

U. Aldemir*

Faculty of Civil Engineering, Division of Applied Mechanics, Istanbul Technical University, 80626 Maslak, Istanbul, Turkey

Received 31 January 2002; accepted 30 September 2002

Abstract

In this paper, the optimal performance of a magnetorheological (MR) damper which is used in a tuned mass damper in reducing the peak responses of a single-degree-of-freedom structure subjected to a broad class of seismic inputs including the harmonic, pulse, artificially generated and recorded earthquake excitations are studied. The optimal semiactive control strategy minimizes an integral norm of the main structure squared absolute accelerations subject to the constraint that the non-linear equations of motion are satisfied and is determined through a numerical solution to the Euler–Lagrange equations. The optimal performance evaluated for an MR damper is compared to an equivalent passive-tuned mass damper with optimized stiffness and damping coefficients. It is shown numerically that the optimal performance of the MR damper is always better than the equivalent passive-tuned mass damper for all the investigated cases and the MR damper has a great potential in suppressing structural vibrations over a wide range of seismic inputs.

1. Introduction

New civil engineering structures tend to be lighter, more slender and have smaller natural damping capacity than those of their older counterparts. This trend has increased the importance of damping technology to mitigate earthquake and wind-induced vibrations. The most widely applied means of suppressing the excessive structural oscillations is the passive-tuned mass damper. This damper consists of a small oscillator attached to a primary system. For the purpose of energy transfer from the primary system to the auxiliary system, which has only a fraction of

*Corresponding author. Civil Eng. Dept., Division of Appl. Mechanics, Istanbul Technical University, 34469 Maslak, Istanbul, Turkey. Fax: +90-212-285-65-87.

E-mail address: aldemiru@itu.edu.tr (U. Aldemir).

0022-460X/03/$ - see front matter
doi:10.1016/S0022-460X(03)00191-3

the primary system mass, the natural vibration period of the damper is selected close enough to the primary system's natural period. The passive-tuned mass damper, otherwise known as vibration absorber was first used by Frahm [1] to suppress the rolling motion of ships. Later, Ormondroyd and Den Hartog [2], Brock [3] and Den Hartog [4] used passive-tuned mass dampers for the reduction of the vibration of single-degree-of-freedom systems. The parameter optimization of the passive-tuned mass dampers were studied by Hahnkam [5], Crandall and Mark [6], Warburton [7] and Tsai and Lin [8]. A list of structures installed with passive-tuned mass dampers has been given by Holmes [9]. However, it is known that passive-tuned mass dampers have some problems: They cannot adapt themselves to changing vibration characteristics of the primary structure and lose their performance in vibration control.

In order to overcome the foregoing drawbacks of passive-tuned mass dampers, the active-tuned mass damper, which requires a prescribed active control algorithm and external power supply to generate the control force that drives the auxiliary mass, was first studied by Morison and Karnopp [10]. However, the first active-tuned mass damper studies in the civil engineering field were made by Lund [11], Chang and Soong [12] and Udwadia and Tabaie [13]. Even though active-tuned mass dampers are more effective than passive ones in vibration control, the dependency of actively controlled systems on the external energy source is a disadvantage since power failure is always possible during strong earthquakes. In addition, their operational costs are high and they need actuators and pumps. A possible alternative device other than passive- and active-tuned mass dampers is a semiactive-tuned mass damper with variable damping and/or stiffness characteristics. It is a new class of tuned mass damper, which has low external energy requirements and low operational costs and it controls the states of the system such that the damping performance is maximized. Hrovat et al. [14] and Abe [15] used semiactive-tuned mass dampers to suppress wind and earthquake-induced vibrations of structures.

Among several semiactive devices, magnetorheological (MR) dampers have a number of attractive characteristics, making them promising for vibration control applications. MR fluids are materials that respond to an applied magnetic field with a dramatic change in rheological behavior and have ability to reversibly change from a free-flowing, linear viscous state to a semi-solid state having a controllable yield strength in milliseconds. MR dampers can be controlled with a low power (e.g., less than 50 W), low voltage (e.g., $\sim$12–24 V), current-driven power supply outputting only $\sim$1–2 A, which could be supplied by batteries [16–19] and are capable of generating large control forces required for full-scale applications. Furthermore, in contrast to servo-valve-based devices, MR dampers do not require intricate moving parts. Recent studies show that MR dampers appear to have significant potential for hazard mitigation [20–28].

However, civil engineering structures incorporating semiactive devices exhibit non-linear behavior and except for relatively few special cases, the mathematical theory of non-linear oscillations provides little help for practical non-linear vibration control problems [29]. As is well known, the optimal control problem of a linear system with respect to a quadratic performance index has a flexible solution which leads to the construction of a linear state regulator when there are no constraints on admissible controls [30–34]. For the case of non-linear non-autonomous dynamical systems, the situation is much more complicated. The difficulties in synthesizing optimal feedback controls for non-linear systems have motivated many researchers to use the formalism of the optimal control theory to derive sub-optimal feedback controllers by obtaining

the approximate solutions to either the two-point boundary-value problem or the Hamilton–Jacobi–Bellman equations.

It is noted here that the evaluation of the exact optimal solutions is important for basically three reasons. Firstly, the ideal best performance achievable by an intrinsically non-linear semiactive device can be obtained only by the exact optimal solution of the corresponding non-linear structure. Secondly, the exact optimal solutions are evaluated in order to check the real optimality of the proposed causal sub-optimal control schemes. Lastly, a careful analysis of the optimal response and control trajectories may help us to improve the proposed algorithms, or to develop better non-linear control rules. This paper is focused basically on the first reason and very little on the third reason.

In this paper, an MR damper is used in a tuned mass damper to suppress the vibration of a base excited single-degree-of-freedom system. The closed-loop dynamics of structures with semiactive control systems are non-linear due to the parametric nature of the control actions. Since these non-linearities prevent the direct evaluation of Laplace transforms, frequency response functions for semiactively controlled investigated system are compiled from the computed time history response to sinusoidal and pulse-type seismic excitations. To be able to measure the optimal performance of MR damper under seismic excitations of random characteristics other than pure harmonic and pure pulse type, a broad class of recorded earthquakes and a simulated earthquake are also used as seismic inputs to the structure.

An optimal, yet non-causal, semiactive controller is derived from the solution to the Euler–Lagrange equations for an MR damper modelled by an algebraic expression. The numerical solution to the Euler–Lagrange equations is obtained using a gradient approach which is a numerical optimization technique [35]. The Euler–Lagrange solution establishes the maximal performance of a dynamically excited and semiactively controlled structure, subjected to the constraints imposed by the particular MR damper. The objective function in the Euler–Lagrange equations is the squared absolute acceleration of the primary structure. The results for optimal semiactive control are compared to those of the equivalent passive-tuned mass damper. Numerical results show that an optimally controlled semiactive-tuned mass damper with an MR damper has a great potential for suppressing base excited vibrations and always outperforms the equivalent passive-tuned mass damper for a wide range of seismic inputs. This will help and encourage the researches to develop better sub-optimal causal control algorithms.

2. Governing equations of motion of the system

This paper examines the optimal response of a single-degree-of-freedom primary structure, to which an auxiliary mass m is attached through a controllable fluid device (i.e., an MR damper) as shown in Fig. 1. The primary system supported by a rigid foundation is assumed to be linear and is represented by a spring in parallel with a linear viscous dash-pot.

The primary structure mass, stiffness and damping coefficients are represented by M, k_1, and c_1, respectively. Structural relative displacements and the ground displacement are denoted by r_1, r_2 and z, respectively. The harmonic ground acceleration is given by

$$\ddot{z}(t) = |Z(\omega)|\sin(\omega t) \tag{1}$$

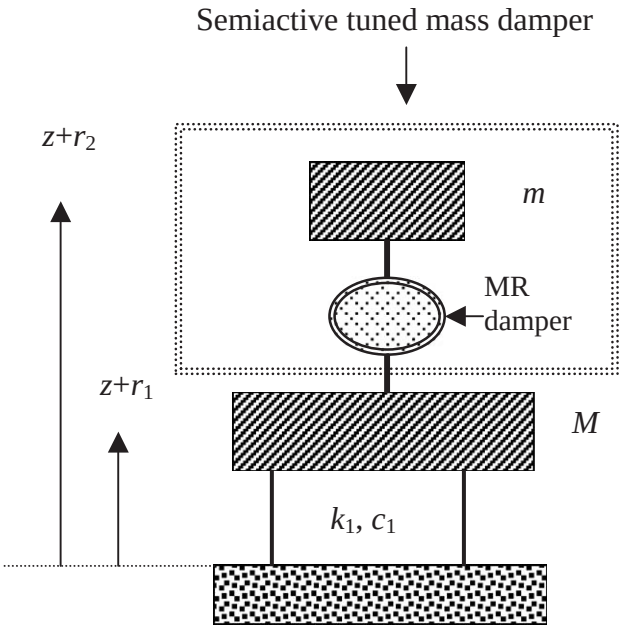

Fig. 1. Idealized vibrating system with semiactive-tuned mass damper.

in which ω is the forcing frequency and the spectral amplitude $|Z(\omega)|$ is generated from the Kanai–Tajimi power spectral density function

$$|Z(\omega)| = \left| \frac{500(\omega/\omega_1)^2}{[1-(\omega/\omega_1)^2 + 2i\rho_1(\omega/\omega_1)]} \frac{1 + 2i\rho_g(\omega/\omega_g)}{[1-(\omega/\omega_g)^2 + 2i\rho_g(\omega/\omega_g)]} \right| \tag{2}$$

and the parameters are $\rho_g = 0.6$, $\rho_1 = 0.6$, $\omega_g = 15.6$ and $\omega_1 = 1.0$ rad/s [36]. The parameters ρ_g, ω_g may be considered as some characteristic damping ratio and characteristic ground frequency, respectively.

For pulse-type excitations, the structure is assumed to be excited by transient pulses of different periods and amplitudes. The symmetric pulse acceleration of period T_{pl} and amplitude A_{pl} is given by

$$\ddot{z}(t) = \begin{cases} (A_1/2)\left[1 - \cos\left(\pi \dfrac{t}{T_1}\right)\right], & 0 < t < T_1, \\ \dfrac{A_{pl} + A_1}{2} \cos\left(\pi \dfrac{t - T_1}{T_{pl}/2 - T_1}\right) + \dfrac{A_1 - A_{pl}}{2}, & T_1 < t < T_{pl}/2, \end{cases} \tag{3}$$

where $A_1 = \ddot{z}(T_1)$ is the first peak (at $t = T_1 = -[(A_1 - A_{pl})T_{pl}/(2A_{pl})]$) and is set to $A_{pl}/1.7$ here. Pulse velocities and pulse displacements are obtained by integrating (3) analytically. The pulse periods and the corresponding amplitudes used in this study are $T_{pl} = 5.0$, 1.67, 1.0, 0.71 and 0.5 s; $A_{pl} = |Z(\omega_{pl})| = 4.920$, 5.377, 5.781, 6.306 and 6.774 m/s^2 where $\omega_{pl} = 2\pi/T_{pl}$. Since the tuned mass dampers are only effective for lightly damped primary structure, the mass, stiffness and the damping coefficients of the investigated primary structure are selected as $M = 100 \times 10^3$ kg,

$k_1 = 400\pi^2 \times 10^3$ N/m, $c_1 = 13 \times 10^3$ N/m/s. The MR damper implemented exhibits controllable stiffness and damping and is modelled by the following algebraic expression with six parameters:

$$f_{MR} = f_{sa} + f_p, \tag{4}$$

where

$$f_{sa} = u[F_{min} + (F_{max} - F_{min})\mathrm{H}(u)] \tanh\left(\frac{r_2 - r_1}{d_d} + \frac{\dot{r}_2 - \dot{r}_1}{v_d}\right), \tag{5}$$

$$f_p = k_0(r_2 - r_1) + c_0(\dot{r}_2 - \dot{r}_1), \tag{6}$$

in which the constant device displacement and velocity parameters d_d and v_d are used to describe the pre-yield behavior of the device, F_{min} and F_{max} are minimum and maximum values for controllable yield force, k_0 and c_0 describe the post-yield behavior and the behavior when $u = 0$, $\mathrm{H}(u)$ is the Heaviside step function of u. These parameters can also be used to represent an ER damper [37–39]. Since the MR device connects a small auxiliary mass m to a much larger primary mass M, the energy flow between the masses can be regulated by the control variable u resulting from a prescribed control scheme. In this paper, the control decision variable u is changed optimally based on the exact solutions of the Euler–Lagrange equations.

When there is no control action ($u = 0$), the semiactive force component becomes zero, $f_{sa} = 0$, and the MR damper force equals the passive force component, $f_{MR} = f_p$. In this case, the auxiliary system serves as a passive-tuned mass damper. The following notations are introduced to define the optimized parameters of the passive-tuned mass damper:

$$\text{Circular frequency of the primal system}: \quad \omega_p = \sqrt{\frac{k_1}{M}}, \tag{7}$$

$$\text{circular frequency of the auxiliary system}: \quad \omega_a = \sqrt{\frac{k_0}{m}}, \tag{8}$$

$$\text{frequency ratio}: \quad \xi = \frac{\omega_a}{\omega_p}, \tag{9}$$

$$\text{mass ratio}: \quad \mu = \frac{m}{M}, \tag{10}$$

$$\text{damping factor}: \quad \varsigma = \frac{c_0}{2m\omega_a}. \tag{11}$$

Parameter optimization of the passive-tuned mass damper results in the following expressions for ξ_{opt} and ς_{opt} [40]:

$$\text{The optimum tuning frequency}: \quad \xi_{opt} = \frac{1}{1+\mu}, \qquad (k_0)_{opt} = m(\xi_{opt})^2(\omega_p)^2, \tag{12}$$

$$\text{The optimum damping factor}: \quad \varsigma_{opt} = \sqrt{\frac{3\mu^3}{8(1+\mu)^3}}, \qquad (c_0)_{opt} = 2m\xi_{opt}\omega_p\varsigma_{opt}. \tag{13}$$

When the control variable $\mu \neq 0$, the auxiliary system works as a semiactive-tuned mass damper. MR damper parameters in this study are $F_{min} = 10$ N, $F_{max} = 100 \times 10^3$ N, $d_d = 0.05$ m, $v_d = 0.04$ m/s.

The non-linear system of dynamical equations of the two-degree-of-freedom structure with an MR damper can be expressed as

$$\dot{\mathbf{x}}(t) = \mathbf{A}\mathbf{x} + \mathbf{g}(\mathbf{x}, u)u + \mathbf{h}\ddot{z}(t), \quad \mathbf{x}(t_0) = \mathbf{0}, \tag{14}$$

where

$$\mathbf{x} = \begin{Bmatrix} r_1 \\ r_2 \\ \dot{r}_1 \\ \dot{r}_2 \end{Bmatrix}, \qquad \mathbf{A} = \begin{bmatrix} 0 & 0 & 1 & 0 \\ 0 & 0 & 0 & 1 \\ -\dfrac{(k_1 + k_0)}{M} & \dfrac{k_0}{M} & -\dfrac{(c_1 + c_0)}{M} & \dfrac{c_0}{M} \\ \dfrac{k_0}{m} & -\dfrac{k_0}{m} & \dfrac{c_0}{m} & -\dfrac{c_0}{m} \end{bmatrix}, \qquad \mathbf{h} = \begin{Bmatrix} 0 \\ 0 \\ -1 \\ -1 \end{Bmatrix}, \tag{15}$$

$$\mathbf{g}(\mathbf{x}, u) = \begin{Bmatrix} 0 \\ 0 \\ [F_{min} + (F_{max} - F_{min})\mathrm{H}(u)] \tanh\left(\dfrac{r_2 - r_1}{d_d} + \dfrac{\dot{r}_2 - \dot{r}_1}{v_d}\right)\left(\dfrac{1}{M}\right) \\ -[F_{min} + (F_{max} - F_{min})\mathrm{H}(u)] \tanh\left(\dfrac{r_2 - r_1}{d_d} + \dfrac{\dot{r}_2 - \dot{r}_1}{v_d}\right)\left(\dfrac{1}{m}\right) \end{Bmatrix}. \tag{16}$$

3. Optimal semiactive control

In this section, firstly optimality conditions for a general non-linear system and then a numerical solution approach to the resulting Euler–Lagrange equations will be presented. Consider a completely observable and controllable non-linear system whose behavior is modelled by a first order system of differential equations, subjected to control actions $\mathbf{u}(t)$, disturbance $\boldsymbol{\rho}(t)$ and with initial conditions $\mathbf{x}_0$, in the state variable form

$$\dot{\mathbf{x}}(t) = \mathbf{f}(\mathbf{x}(t), \mathbf{u}(t), \boldsymbol{\rho}(t), t), \quad \mathbf{x}(t_0) = \mathbf{x}_0, \ \ \mathbf{x} \in R^n, \ \ \mathbf{u} \in R^m, \ \ \boldsymbol{\rho} \in R^s, \tag{17}$$

where $\mathbf{x}(t)$ is the state vector and the vector $\mathbf{f}$ is a given function of the state vector $\mathbf{x}(t)$, the control vector $\mathbf{u}(t)$, disturbance vector $\boldsymbol{\rho}(t)$ and the time t. The most general cost function to be minimized is defined as

$$J = \phi[\mathbf{x}(t_f), \boldsymbol{\rho}(t_f), t_f] + \int_{t_0}^{t_f} L[\mathbf{x}(t), \mathbf{u}(t), \boldsymbol{\rho}(t), t]\,\mathrm{d}t, \tag{18}$$

where ϕ is a scalar algebraic function of the final state $\mathbf{x}(t_f)$, final disturbance $\boldsymbol{\rho}(t)$and time t, and the integrand L is scalar and generally called the Lagrangian. However, since the disturbance $\boldsymbol{\rho}(t)$ is assumed to be known a priori function of time in the whole control interval $[0, t_f]$, the system dynamics (17) and the cost function (18) can be expressed as

$$\dot{\mathbf{x}}(t) = \mathbf{f}(\mathbf{x}(t), \mathbf{u}(t), t), \quad \mathbf{x}(t_0) = \mathbf{x}_0, \ \ \mathbf{x} \in R^n, \ \ \mathbf{u} \in R^m, \tag{19}$$

$$J = \phi[\mathbf{x}(t_f), t_f] + \int_{t_0}^{t_f} L[\mathbf{x}(t), \mathbf{u}(t), t]\,\mathrm{d}t, \tag{20}$$

respectively, without loss of generality [35,41]. Since the system given by Eq. (19) is forced by $\boldsymbol{\rho}(t)$ and the right-hand sides depend explicitly on time t [42], the system is non-autonomous and Eq. (19) represents the non-autonomous systems which are studied in this paper.

The minimization of the cost function (20) subjected to the constraint of the dynamical system equation (19) employs an augmented cost function

$$J_A = \phi[\mathbf{x}(t_f), t_f] + \int_0^{t_f} [L(\mathbf{x}(t), \mathbf{u}(t), t) + \boldsymbol{\lambda}^{\mathrm{T}}(t)(\mathbf{f}(\mathbf{x}(t), \mathbf{u}(t), t) - \dot{\mathbf{x}}(t))]\,\mathrm{d}t, \tag{21}$$

where the Lagrange multipliers $\boldsymbol{\lambda}(t)$, whose purpose is to ensure that the dynamical system equation (19) is taken into account in the minimization process, is commonly referred to as the costate vector. To summarize the most important results, introduce the Hamiltonian

$$H(\mathbf{x}(t), \mathbf{u}(t), \boldsymbol{\lambda}(t), t) = L(\mathbf{x}(t), \mathbf{u}(t), t) + \boldsymbol{\lambda}^{\mathrm{T}}\mathbf{f}(\mathbf{x}(t), \mathbf{u}(t), t). \tag{22}$$

Substituting Eq. (22) into Eq. (21), J_A can also be rewritten as

$$J_A = \phi[\mathbf{x}(t_f), t_f] + \int_0^{t_f} [H(\mathbf{x}(t), \mathbf{u}(t), \boldsymbol{\lambda}(t), t) - \boldsymbol{\lambda}^{\mathrm{T}}(t)\dot{\mathbf{x}}(t)]\,\mathrm{d}t. \tag{23}$$

Setting the first variation of J_A to zero results in the following necessary conditions of optimality known as the Euler–Lagrange equations [35]:

$$\dot{\boldsymbol{\lambda}}(t) = \left(-\frac{\partial H}{\partial \mathbf{x}}\right)^{\mathrm{T}} = -\left[\frac{\partial \mathbf{f}(\mathbf{x}, \mathbf{u}, t)}{\partial \mathbf{x}}\right]^{\mathrm{T}} \boldsymbol{\lambda}(t) - \left[\frac{\partial L(\mathbf{x}, \mathbf{u}, t)}{\partial \mathbf{x}}\right]^{\mathrm{T}}, \quad t_0 < t < t_f, \tag{24}$$

$$\frac{\partial H}{\partial \mathbf{u}} = \boldsymbol{\lambda}^{\mathrm{T}}(t)\frac{\partial \mathbf{f}(\mathbf{x}, \mathbf{u}, t)}{\partial \mathbf{u}} + \frac{\partial L(\mathbf{x}, \mathbf{u}, t)}{\partial \mathbf{u}} = \mathbf{0}, \quad t_0 < t < t_f, \tag{25}$$

$$\left[\frac{\partial \phi[\mathbf{x}(t_f), t_f]}{\partial \mathbf{x}} - \boldsymbol{\lambda}(t_f)\right]^{\mathrm{T}} \delta\mathbf{x}(t_f) + \left[H(\mathbf{x}(t_f), \mathbf{u}(t_f), \boldsymbol{\lambda}(t_f), t_f) + \frac{\partial \phi[\mathbf{x}(t_f), t_f]}{\partial t}\right]\delta t_f = 0. \tag{26}$$

The system of equations given by the state equation (19), the costate equation (24), the gradient equation of the Hamiltonian (25) and Eq. (26) for boundary conditions provide the necessary conditions, but not the sufficient conditions in general, for the optimal solution for $\mathbf{x}(t)$, $\mathbf{u}(t)$ and $\boldsymbol{\lambda}(t)$. Eq. (26) implies that the final state $\mathbf{x}(t)$ and the final time t_f are free. As a special case, if the final time t_f is fixed and the algebraic function ϕ is assumed to be zero, then the final boundary condition for the costate equation (24) is obtained as $\boldsymbol{\lambda}(t_f) = \mathbf{0}$. Eq. (25) is not valid when there are restrictions on the set of admissible controls $\mathbf{u}(t)$ such as actuator saturations.

Eqs. (19) and (24) define a two-point boundary-value problem since $\mathbf{x}(t)$ is specified at $t = t_0$ and $\boldsymbol{\lambda}(t)$ is specified at $t = t_f$. The gradient equation of the Hamiltonian (25) involves the costate vector $\boldsymbol{\lambda}(t)$, which is determined by integrating the costate equation (24) backward in time. For the non-autonomous systems such as earthquake and wind excited structures under control, disturbance must be known a priori in control interval $[t_0, t_f]$. Even though the earthquake excitation can be measurable at the current time t, it cannot be known a priori. Consequently, only sub-optimal solutions can be obtained for these type of structures. Simultaneous solution of the coupled state and costate equations throughout the control interval can be complicated for non-autonomous

systems. The method of successive approximation is used here to converge upon the optimal controls, state and costate trajectories for a general non-linear case.

4. Numerical solution of the Euler–Lagrange equations

To obtain the optimal state trajectory $\mathbf{x}(t)$, costate trajectory $\boldsymbol{\lambda}(t)$ and the corresponding control actions $\mathbf{u}(t)$, Eqs. (19) and (24) are solved successively. In this paper, a gradient approach in which the state and costate equations are solved based on the iterations made on the control function $\mathbf{u}(t)$ is used. The first step of the approach is to specify initial conditions and guess an initial control trajectory $\mathbf{u}_0(t)$ for the control interval $[t_0, t_f]$. Forward integration of the state equation (19) in time gives the corresponding state trajectory $\mathbf{x}_0(t)$. To evaluate the numerical solution of the system sensitivity matrices $\partial\mathbf{f}/\partial\mathbf{x}$ and $\partial\mathbf{f}/\partial\mathbf{u}$ and Lagrangian gradients $\partial L/\partial\mathbf{x}$ and $\partial L/\partial\mathbf{u}$ for a given trial control trajectory $\mathbf{u}_0(t)$ and the corresponding state trajectory $\mathbf{x}_0(t)$; the following Jacobian matrix is used:

$$\frac{\partial\mathbf{F}(t)}{\partial\mathbf{v}} = \begin{bmatrix} \left(\dfrac{\partial\mathbf{f}(t)}{\partial\mathbf{x}}\right)_{nxn} & \left(\dfrac{\partial\mathbf{f}(t)}{\partial\mathbf{u}}\right)_{nxm} \\ \left(\dfrac{\partial L(t)}{\partial\mathbf{x}}\right)_{1xn} & \left(\dfrac{\partial L(t)}{\partial\mathbf{u}}\right)_{1xm} \end{bmatrix}, \tag{27}$$

where

$$\mathbf{F} = \begin{Bmatrix} \dot{\mathbf{x}} \\ \dot{J} \end{Bmatrix} = \begin{bmatrix} \mathbf{f}(\mathbf{x}(t), \mathbf{u}(t), t) \\ L(\mathbf{x}(t), \mathbf{u}(t), t) \end{bmatrix}, \qquad \mathbf{v} = \begin{Bmatrix} \mathbf{x} \\ \mathbf{u} \end{Bmatrix}. \tag{28}$$

It should be noted here that these partial derivatives in Eq. (27) can only be calculated for specified values of $\mathbf{x}(t) = \mathbf{x}_0(t)$ and $\mathbf{u}(t) = \mathbf{u}_0(t)$. Upon calculating $\partial\mathbf{f}/\partial\mathbf{x}$, $\partial\mathbf{f}/\partial\mathbf{u}$, $\partial L/\partial\mathbf{x}$ and $\partial L/\partial\mathbf{u}$ numerically from Eqs. (27) and (28), the costate vector $\boldsymbol{\lambda}_0(t)$ is obtained from backward integration of Eq. (24), and $\partial H/\partial\mathbf{u}$ is found from Eq. (25). The control trajectory $\mathbf{u}_k(t)$ is then updated in the direction of steepest descent

$$\mathbf{u}_{k+1}(t) = \mathbf{u}_k(t) - K_k \frac{\partial H}{\partial\mathbf{u}_k}(t), \tag{29}$$

where K_k is a scalar gradient gain. Appropriate choice of the update gain K_k is important to achieve a rapid convergence to the optimal control trajectory. In this paper, the gradient gain which maximizes the reduction in J is found using a bisection method. The iterations continue until the cost function J is not reduced significantly, or until $\partial H/\partial\mathbf{u}$ becomes small as compared to $\mathbf{u}_k(t)$.

5. Generation of the simulated earthquake

An homogeneous random process with zero mean and spectral density $S(\omega)$ can be simulated by the following series as [43]:

$$f(t) = \sum_{m=1}^{N} A_m \cos(\omega_m t + \phi_m), \tag{30}$$

where

$$A_m = [2S(\omega_m)\delta\omega]^{1/2}, \qquad \omega_m = m\delta\omega, \;\; \delta\omega = \omega_u/N, \;\; \omega_u = 2\pi/\delta t, \tag{31}$$

in which ϕ_m denotes the angles distributed uniformly between 0 and 2π; ω_u is the upper cut-off frequency and N is a sufficiently large positive number. In order to take advantage of the fast Fourier transform (FFT), Eq. (30) can be written in the following form:

$$f(p\delta t) = \mathrm{Re}\left\{\sum_{n=0}^{M-1} B_n e^{inp2\pi/M}\right\}, \quad p = 0, 1, 2, ..., M-1, \;\; M \geqslant 2N, \tag{32}$$

where

$$B_n = \sqrt{2}[2S(n\delta\omega)\delta\omega]^{1/2} e^{i\phi_n}. \tag{33}$$

Instead of using Eq. (30) including just summation of cosines, the FFT technique can be used on Eq. (32), which results in the reduction of computer time. To be able to take advantage of FFT technique, M must be an integer power of 2 and given as $M = 2^{\mu}$ where μ is a positive integer. In this study, artificial ground acceleration is modelled as a uniformly modulated non-stationary random process with zero mean by multiplying a deterministic non-negative modulating function $s(t)$ and a stationary zero mean Gaussian process $f(t)$ (obtained from Eq. (32)) with a power spectral density function $S(\omega)$ given below

$$S(\omega) = \frac{1 + 4\xi_g^2(\omega/\omega_g)^2}{[1-(\omega/\omega_g)^2]^2 + 4\xi_g^2(\omega/\omega_g)^2} S_0^2, \tag{34}$$

where the parameters ω_g, ξ_g and S_0 related to the intensity and the characteristics of earthquakes at a particular geological location represent the predominant frequency, damping factor of subsoil layers and the power spectrum at $\omega = 0$, respectively. The selected modulating function is given as

$$\begin{aligned} s(t) &= (t/t_1)^2, \;\; 0 \leqslant t \leqslant t_1, \\ s(t) &= 1, \;\; t_1 \leqslant t \leqslant t_2, \\ s(t) &= e^{[-c(t-t_2)]}, \;\; t > t_2, \end{aligned} \tag{35}$$

in which t_1, t_2 and c are usually given by regression analysis using many strong-motion records. They reflect the shape and the duration of the earthquake. The specific values for these parameters used in this paper are as follows:

$$\begin{aligned} &t_1 = 4\,\mathrm{s}, \quad t_2 = 14\,\mathrm{s}, \quad c = 0.26\,\mathrm{s}^{-1}, \quad \omega_g = 18.85\,\mathrm{rad/s}, \\ &\xi_g = 0.65 \quad \text{and} \quad S_0^2 = 0.00045\,\mathrm{m}^2/\mathrm{s}^2. \end{aligned} \tag{36}$$

6. Numeric analysis

Even though an algebraic model is used in this paper for the MR damper, there are many other hysteretic models developed independent of each other based on different behavioral, physical, or mathematical motivations [44]. For instance, Bingham viscoplastic model [45] consists of a viscous damping term in parallel with a yield force controllable by a voltage signal applied to the

electromagnets in the MR damper. Bouc–Wen model [46,47] is another model used for MR dampers [48] and can exhibit a wide variety of hysteretic behavior. Spencer et al. [48] also proposed a phenomenological model. Optimal performance achievable for each MR model can be obtained for several inputs of different characteristics using the optimal control scheme given in Sections 3 and 4 and then the resulting optimal performances can be used to compare the model performances, or using a constraint optimization scheme, the appropriate parameters for each model can be determined. However, since this paper is basically focused on the optimal performance of semiactive-tuned mass dampers incorporating an MR damper modelled by an algebraic expression with specified parameters, comparison of optimal performances of different MR models is beyond the scope of this paper.

Because of the Heaviside step function in Eq. (16), analytical expressions for the frequency response function cannot be obtained. However, for both the sinusoidal and the pulse-type excitations defined previously, frequency response functions for semiactively controlled structure can be constructed by numerically integrating the system equations and plotting the ratio of a response amplitude to the excitation amplitude as a function of frequency ratio ($\omega/\omega_p = \omega_{pl}/\omega_p$). In order to ensure that a harmonic steady state is achieved, the final time t_f is selected as $t_f = \max[10\pi/\omega_p, 10\pi/\omega]$ for harmonic excitations. For pulse-type excitations, the final time t_f for the performance index is selected as $t_f = 2T_{pl}$. To compare the performances of the passive-tuned mass damper and the optimal semiactive control in reducing the peak acceleration, velocity and displacement of the primary structure, the non-dimensional acceleration, velocity and displacement performance parameters are defined as

$$p_a = \frac{\{T_a(\omega)\}_{osa}}{\{T_a(\omega)\}_{ptd}}, \quad p_v = \frac{\{T_v(\omega)\}_{osa}}{\{T_v(\omega)\}_{ptd}}, \quad p_d = \frac{\{T_d(\omega)\}_{osa}}{\{T_d(\omega)\}_{ptd}}, \tag{37}$$

where frequency-dependent acceleration, velocity and displacement response transmissibility ratios $T_a(\omega)$, $T_v(\omega)$ and $T_d(\omega)$ are expressed as [36,49]

$$T_a(\omega) = \frac{\max|\ddot{r}_1 + \ddot{z}|}{\max|\ddot{z}|}(\omega), \quad T_v(\omega) = \frac{\max|\dot{r}_1 + \dot{z}|}{\max|\dot{z}|}(\omega), \quad T_d(\omega) = \frac{\max|r_1|}{\max|z|}(\omega). \tag{38}$$

In Eq. (37), the subscripts '$_{osa}$' and '$_{ptd}$' denote the optimal semiactive control and the passive-tuned mass damper, respectively. The smaller values of performance parameters indicate an improvement in the efficiency of MR damper under optimal semiactive control. In the numerical analysis, the optimized stiffness ($(k_0)_{opt}$) and damping ($(c_0)_{opt}$) coefficients of the passive-tuned mass damper are calculated from Eqs. (12) and (13) and the mass ratios (μ) are selected as 0.01, 0.05, 0.15, 0.30 and 0.50. The Lagrangian $L(\mathbf{x}(t), u(t), t)$ of the integral cost function (20) is selected as the square of the absolute acceleration of the main structure and the terminal cost ϕ is assumed to be zero.

$$\begin{aligned} &L(\mathbf{x}(t), u(t), t) \\ &\quad = [\ddot{r}_1(t) + \ddot{z}(t)]^2 \\ &\quad = \left\{ -\frac{1}{M}\left[(k_1 + k_0) r_1 + (c_1 + c_0)\dot{r}_1 + (F_{min} + (F_{max} - F_{min})\mathrm{H}(u))\tanh\left(\frac{r_2 - r_1}{d_d} + \frac{\dot{r}_2 - \dot{r}_1}{v_d} \right) \right] \right\}^2. \end{aligned} \tag{39}$$

To be able to obtain the optimal control trajectories for MR damper, the iterative procedure described previously is started with $u_0(t) = 1$ for all cases.

For the comparison of the performances of the passive-tuned mass damper and the optimal semiactive control in reducing the peak response of the primary structure, frequency-dependent non-dimensional acceleration, velocity and displacement performance parameters given by Eq. (37) are calculated for harmonic excitations defined previously and shown in Figs. 2–4, respectively.

As seen from these figures, an optimally controlled MR damper can outperform its equivalent passive-tuned mass damper in terms of the acceleration, velocity and displacement performances since the calculated performance parameters corresponding to different mass and frequency ratios are less than one for all the investigated cases. However, for all the investigated mass ratios, optimal acceleration, velocity and displacement performances of the semiactive-tuned mass damper with MR damper at low frequencies ($\omega/\omega_p \approx 0.2$) are not as effective as the resonance and high frequency ($\omega/\omega_p \approx 2$) performances. Figs. 2–4 show that the mass ratios in the range $\mu = 0.05$–0.15 result in the best acceleration, velocity and displacement performances at resonance at the same time. These mass ratios also result in almost the best acceleration and velocity performances at high frequencies. This result indicates that the appropriate mass ratio to achieve a good acceleration and velocity performances at both resonance and high frequencies should be in the range $\mu = 0.05$–0.15. It should be noted here that the best displacement performance at high frequencies can be obtained for $\mu = 0.30$–0.50. However, in general, it is difficult to say that the high mass ratios result in good performance especially for acceleration.

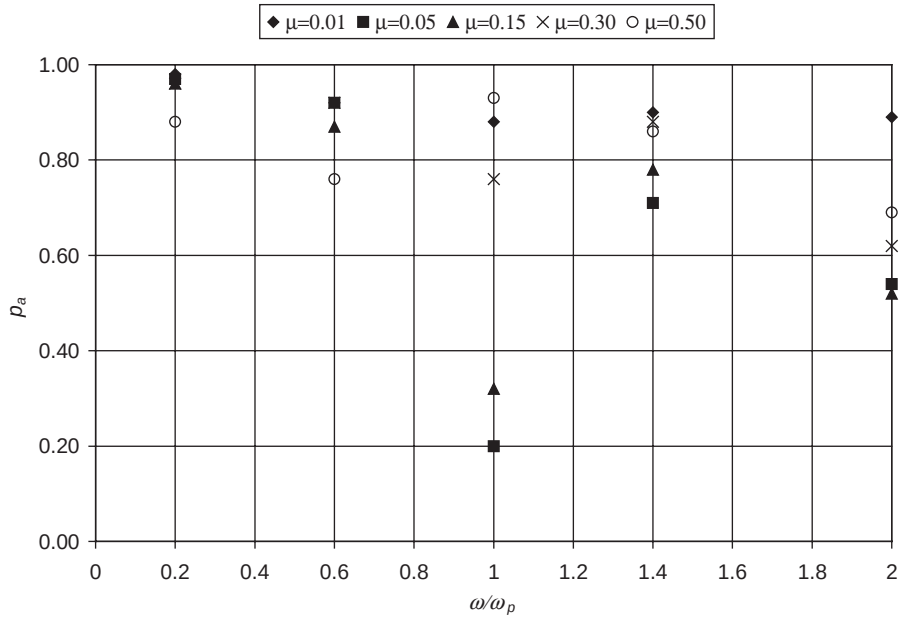

Fig. 2. Variation of acceleration performance parameter (p_a) with forcing frequency ratio (ω/ω_p) for different mass ratios μ (Harmonic excitation).

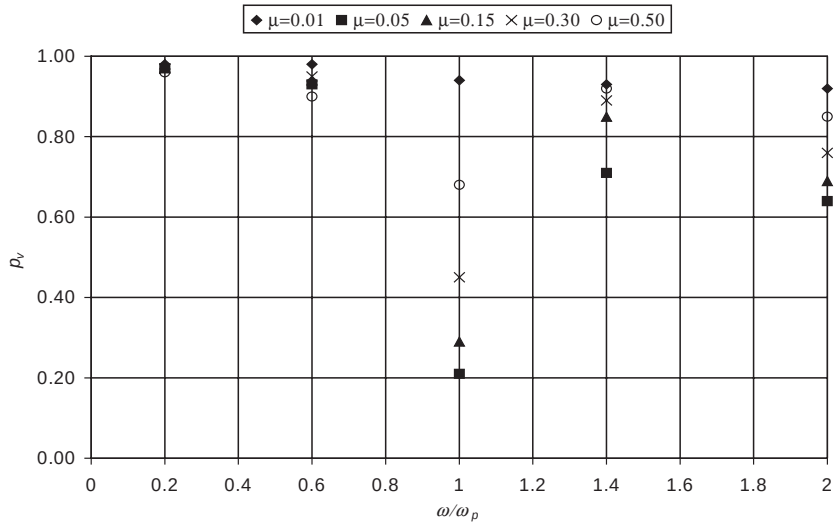

Fig. 3. Variation of velocity performance parameter (p_v) with forcing frequency ratio (ω/ω_p) for different mass ratios μ (Harmonic excitation).

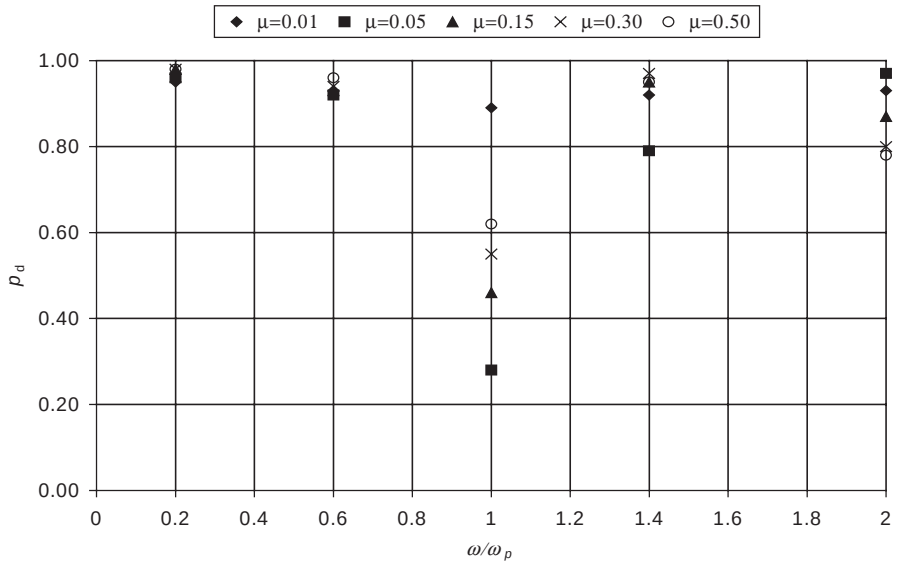

Fig. 4. Variation of displacement performance parameter (p_d) with forcing frequency ratio (ω/ω_p) for different mass ratios μ (Harmonic excitation).

Since the primary structure M will be subjected to large amplitudes of response at resonance, in which the forcing frequency ω is close to the natural frequency of the primary structure ω_p, ($\omega/\omega_p \approx 1$), one is mainly interested in the resonance response of the investigated structure with MR damper under optimal semiactive control. Fig. 5 presents the performance percentages of the optimally controlled MR damper at resonance compared to passive-tuned mass damper. For

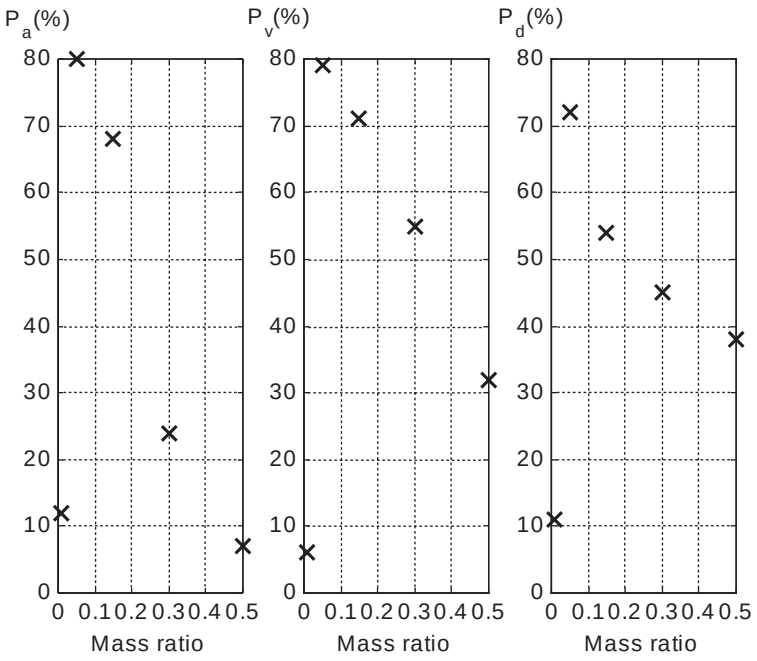

Fig. 5. Resonance performance of the optimal semiactive-tuned mass damper compared to equivalent passive-tuned mass damper with the optimized parameters (Harmonic excitation).

example, 80% performance for P_a means that optimal semiactive control results in 80% reduction in the peak acceleration response of the main structure compared to equivalent passive-tuned mass damper. Consequently, as the performance parameter decreases, the corresponding performance percentage increases.

As shown in Fig. 5, when the mass ratio is small ($\mu = 0.01$), the general performance is not very high. If the mass ratio is between $\mu = 0.05$ and 0.15, the system reaches the maximum performance for acceleration, velocity and displacement at the same time. Beyond this point, performance parameters start to decrease. So, the choice of the appropriate mass ratio for the best acceleration, velocity and displacement simultaneous resonance performance of the harmonic excitation is very important. Otherwise, the performance level will decrease significantly while the optimal semiactive case is still better than the equivalent passive case. However, it should also be noted that the best simultaneous velocity and displacement performance at resonance can also be achieved in a wider mass ratio range $\mu = 0.05$–0.50. The frequency-dependent non-dimensional acceleration, velocity and displacement performance parameters calculated for pulse excitations are shown in Figs. 6–8, respectively.

As in the case of harmonic loading, performance parameters less than one indicate that the MR damper outperforms its equivalent passive-tuned mass damper for all the investigated cases corresponding to different mass and frequency ratios, provided that the control parameter u is regulated optimally while the performance levels may vary for each of the cases. As shown in Figs. 6–8, the optimal performance parameters for all the investigated mass ratios, especially the acceleration and displacement performances, are much better in the frequency range

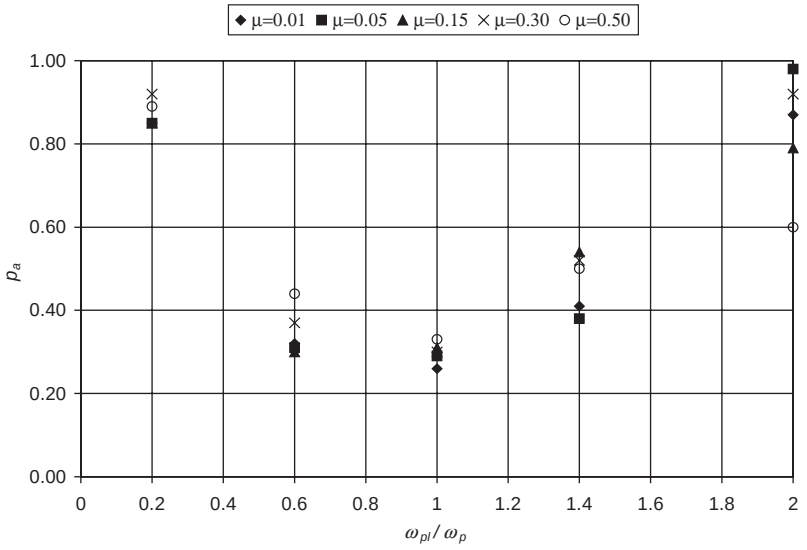

Fig. 6. Variation of acceleration performance parameter (p_a) with forcing frequency ratio (ω_{pl}/ω_p) for different mass ratios μ (pulse excitation).

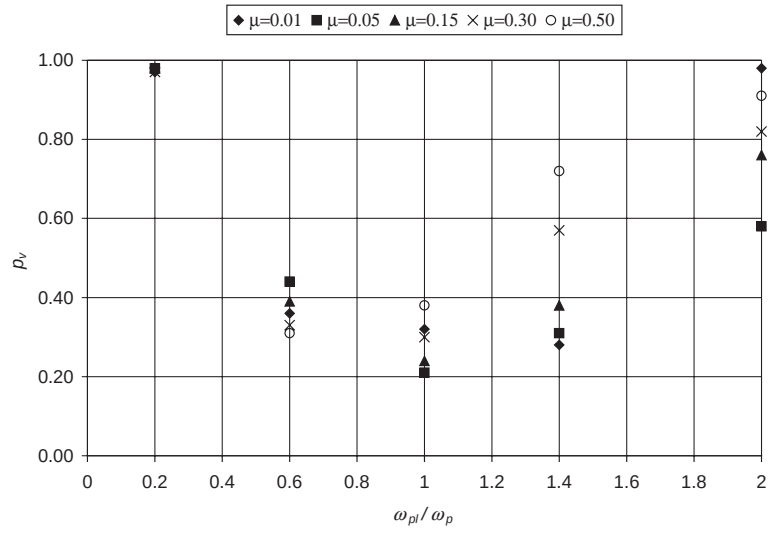

Fig. 7. Variation of velocity performance parameter (p_v) with forcing frequency ratio (ω_{pl}/ω_p) for different mass ratios μ (pulse excitation).

$0.6 \leqslant (\omega_{pl}/\omega_p) \leqslant 1.4$ than those obtained at low ($\omega_{pl}/\omega_p \approx 0.2$) and high ($\omega_{pl}/\omega_p \approx 2$) frequencies. It is also noted that the best performance for pulse excitation in the range $0.6 \leqslant (\omega_{pl}/\omega_p) \leqslant 1.4$ is achieved at resonance which is very important for vibration control applications. At low frequencies, the general performance is low and the mass ratio has almost no effect on the performance. At high frequencies, the best acceleration performance is obtained for $\mu = 0.50$ while

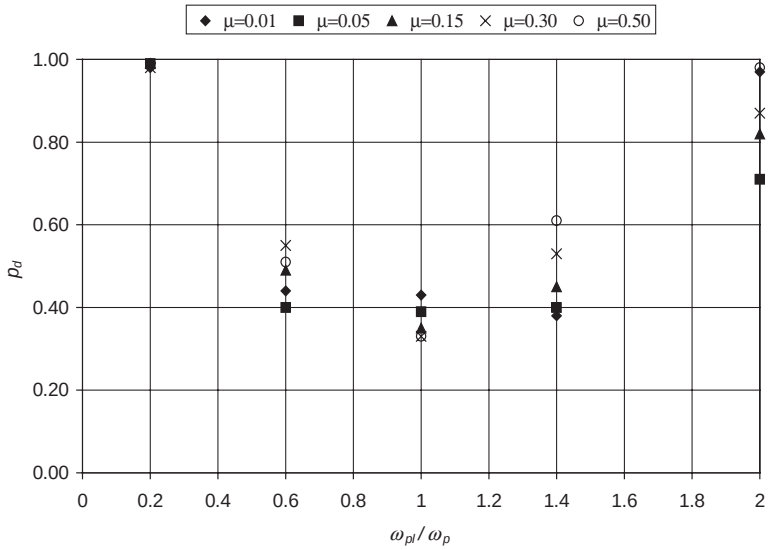

Fig. 8. Variation of displacement performance parameter (p_d) with forcing frequency ratio (ω_{pl}/ω_p) for different mass ratios μ (pulse excitation).

the best velocity and displacement performances are obtained for $\mu = 0.05$. The mass ratio has no significant effect on the performances in the range $0.6 \leqslant (\omega_{pl}/\omega_p) \leqslant 1.4$ except for velocity performance at $(\omega_{pl}/\omega_p) = 1.4$. Performance percentages at resonance for pulse excitations are shown in Fig. 9.

It is clear that the general performance, especially the acceleration performance, is not effected by the change in the mass ratio compared to harmonic excitation case. The most effective μ range for acceleration and velocity can be selected as $\mu = 0.01$–0.30 and 0.15–0.50 for the displacement. The minimum performance percentage is 57% for the displacement. So, the choice of the most appropriate mass ratio at resonance for pulse excitations does not seem to be as important as in harmonic case since the performance percentages for all μ are very high at resonance.

It has been shown that the optimally controlled MR damper implemented in a semiactive-tuned mass damper outperforms, especially at resonance, equivalent passive-tuned mass damper for harmonic and pulse-type excitations. Since it is known that the earthquakes are naturally neither purely impulsive nor harmonic, the optimal earthquake performance of MR damper should also be investigated for several earthquakes to include the effect of the random characteristics of the input disturbance. For this purpose, eight recorded earthquakes: RinaldiEW (Northridge Earthquake; January 17, 1994; Rinaldi Station), RinaldiNS (Northridge Earthquake; January 17, 1994; Rinaldi Station), SylmarEW (Northridge Earthquake; January 17, 1994; Sylmar Station), SylmarNS (Northridge Earthquake; January 17, 1994; Sylmar Station), KobeEW (Kobe Earthquake; January 17, 1996; Kobe Station), KobeNS (Kobe Earthquake; January 17, 1996; Kobe Station), ElcentroEW (Imperial Valley Earthquake; May 18, 1940; El Centro Station), ElcentroNS (Imperial Valley Earthquake; May 18, 1940; El Centro Station) and a synthetic earthquake generated using FFT technique, which are shown in Fig. 10 are used as seismic inputs to the structure.

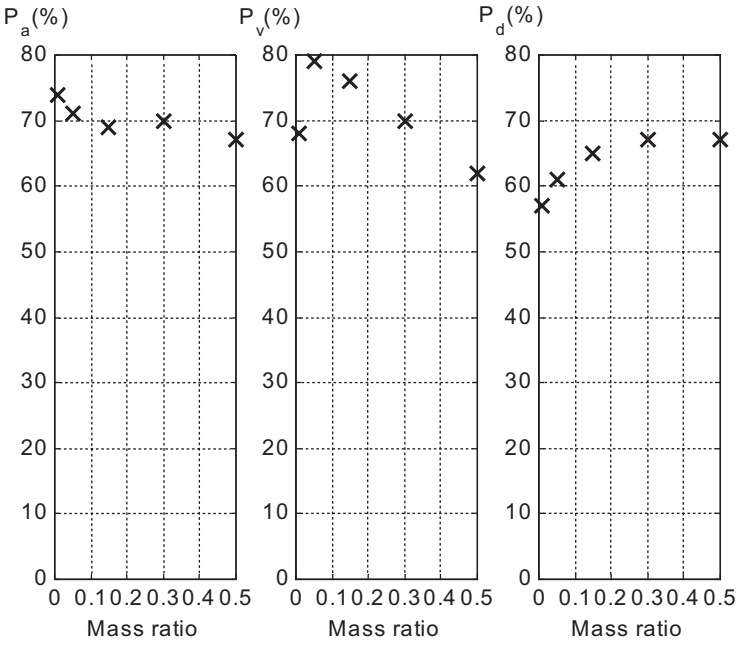

Fig. 9. Resonance performance of the optimal semiactive-tuned mass damper compared to equivalent passive-tuned mass damper with the optimized parameters (pulse excitation).

Performance percentages of the optimal semiactive-tuned mass damper compared to equivalent passive-tuned mass damper for these earthquakes are illustrated in Figs. 11–19. As presented in Figs. 11–19, even though the optimally controlled semiactive-tuned mass damper with MR damper outperforms its equivalent passive-tuned mass damper for the investigated earthquake inputs, the performance levels are different. For instance, the best acceleration, velocity and displacement performance percentages for the simulated earthquake (Fig. 11) are 18%, 16% and 15%, respectively, while the corresponding performance percentages for KobeEW (Fig. 12) and SylmarNS (Fig. 14) earthquakes are 60%, 49%, 46% and 50%, 27%, 47%, respectively.

For the KobeEW earthquake, all the performance levels increase until μ reaches 0.15 and then they start to decrease. The best performances for acceleration, velocity and displacement are achieved at the same mass ratio $\mu = 0.15$ which is optimal for this earthquake and the corresponding time responses of the primary structure are demonstrated in Fig. 20 just for illustrative purposes.

Optimal MR performance for the KobeNS earthquake (Fig. 13) is similar to that of the KobeEW earthquake while the optimal mass ratio is $\mu = 0.30$. In the SylmarNS earthquake case (Fig. 14), all the performance percentages increase almost linearly with μ and we get the best performance for acceleration, velocity and displacement for the largest mass ratio $\mu = 0.50$. The SylmarEW case (Fig. 15) is similar to the KobeNS case and the optimal mass ratio is $\mu = 0.30$. For the ElcentroEW input (Fig. 16), the optimal mass ratio $\mu = 0.30$ for the acceleration can be assumed to be optimal also for velocity and displacement. Even though the optimal mass ratios corresponding to the acceleration, velocity and displacement are the same for the previous earthquakes, different optimal mass ratios are obtained for the ElcentroNS earthquake (Fig. 17);

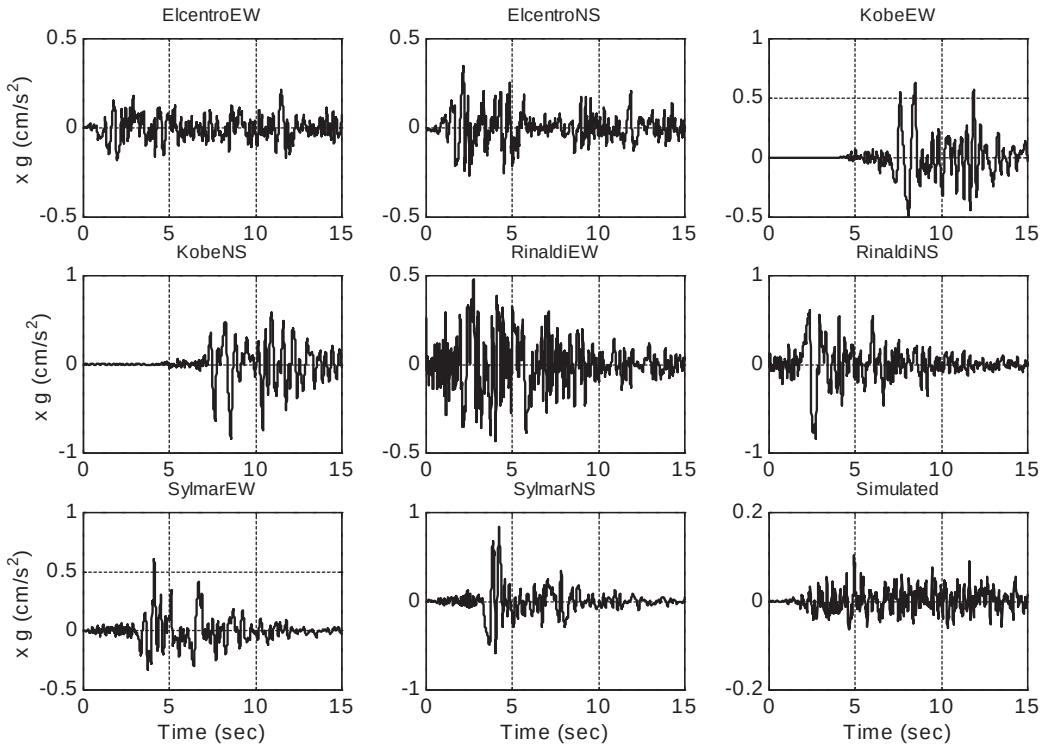

Fig. 10. Recorded and generated seismic inputs.

optimal mass ratios for the acceleration, velocity and displacement are 0.50, 0.30 and 0.15, respectively. The optimal mass ratio for the RinaldiEW earthquake (Fig. 18) is $\mu = 0.30$. Lastly, in the RinaldiNS case (Fig. 19), the optimal mass ratios for the acceleration and displacement are the same and equal to $\mu = 0.30$, but for velocity $\mu = 0.50$. For the previous earthquake cases investigated, the optimal mass ratios are obtained in the range $\mu = 0.15$–0.50 while the general performance at small mass ratios $\mu = 0.01$–0.05 are low. However, in the last case, while the performance at $\mu = 0.05$ is low, all the performance percentages at $\mu = 0.01$ are very high compared to previous results for $\mu = 0.01$. It is also noted that the optimal acceleration performance percentage is always greater than the velocity and displacement performance. It is an expected result because the selected performance measure to be minimized is the squared absolute acceleration of the primary structure.

The above given results show that the optimal MR damper performance is strongly related to the earthquake characteristics. A mass ratio which is optimal for one earthquake may result in a low performance for another earthquake, or the optimal mass ratio values corresponding to the same earthquake may also be different for acceleration, velocity and displacement. Exact optimal values can only be calculated based on the exact a priori knowledge of the earthquake which is not possible in practice. However, numerical results indicate that in general, the optimal mass ratios are in the range $\mu = 0.15$–0.50, while the semiactive-tuned mass damper still outperforms equivalent passive damper even for non-optimal mass ratios. Assuming that the optimal design parameters are almost known, one should decide on an appropriate causal sub-optimal control

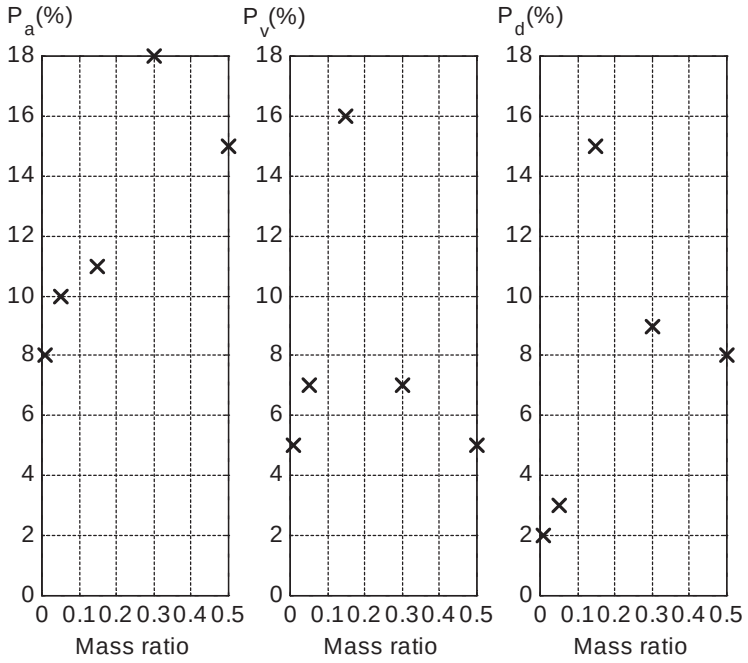

Fig. 11. Performance of the optimal semiactive-tuned mass damper compared to equivalent passive-tuned mass damper for simulated earthquake.

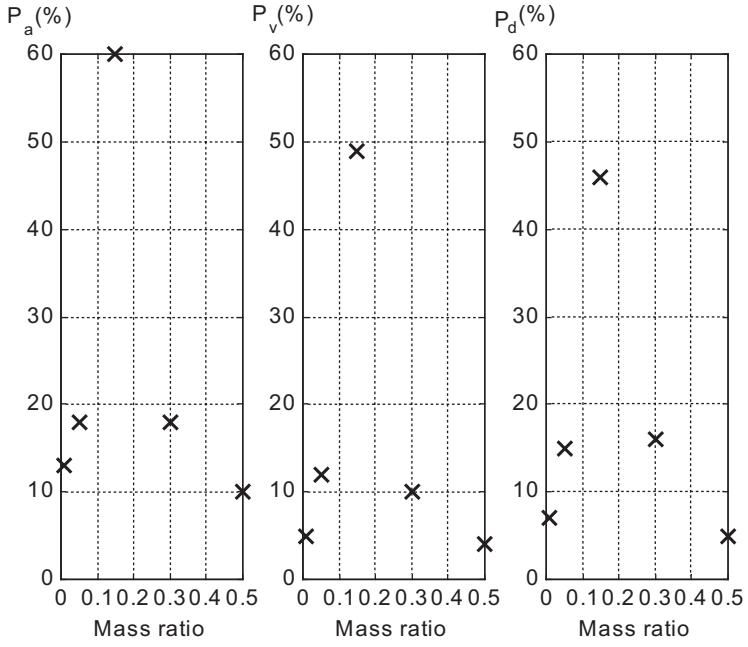

Fig. 12. Performance of the optimal semiactive-tuned mass damper compared to equivalent passive-tuned mass damper for KobeEW earthquake.

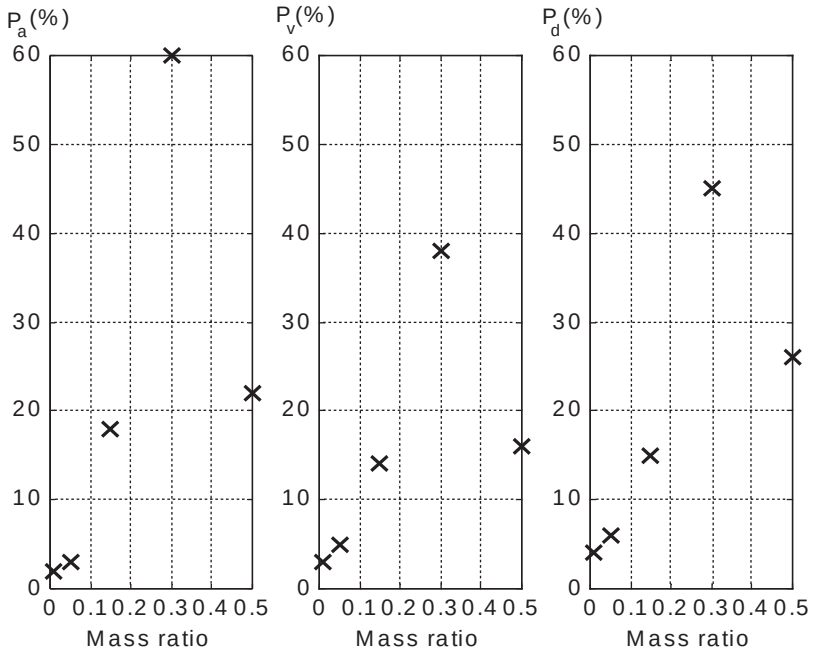

Fig. 13. Performance of the optimal semiactive-tuned mass damper compared to equivalent passive-tuned mass damper for KobeNS earthquake.

scheme applicable to non-linear structure. It is concluded from the previous results that the proposed control schemes must take into account the unknown disturbance, or at least the near future disturbance information through observers.

Exact optimal solutions may help one to understand how to include the disturbance into control schemes. The effectiveness of the most of the proposed active and semiactive control laws are evaluated and measured by comparing the peak controlled and uncontrolled (or passive) structural responses. However, the optimality level of the proposed control scheme must also be measured by comparing with the exact optimal solutions. Numerical solution of the Euler–Lagrange equations is easy for the linear systems with quadratic cost function because all of the needed partial derivatives are independent of the state and control perturbations [35]. But, because the intrinsically non-linear nature of semiactive devices, semiactively controlled structures are non-linear and the corresponding state and costate equations are coupled. Since the numerical solution of the Euler–Lagrange equations for non-linear systems is not as easy as linear systems, exact optimal solutions of non-linear systems are not given in general. However, there are some important works that use the optimal active control laws to calculate the control parameter of the semiactive device [44,50]. The implementable optimal active control laws such as classical closed-loop control and instantaneous optimal control are in fact not truly optimal in the sense that they ignore future disturbances [51,52]. So, although it is known that the exact optimal solutions cannot be implemented, based on the detailed analysis of the optimal response and control trajectories and the possible relations between them, it may be possible to get some important hints from the optimal data in developing some implementable very simple causal rules in the

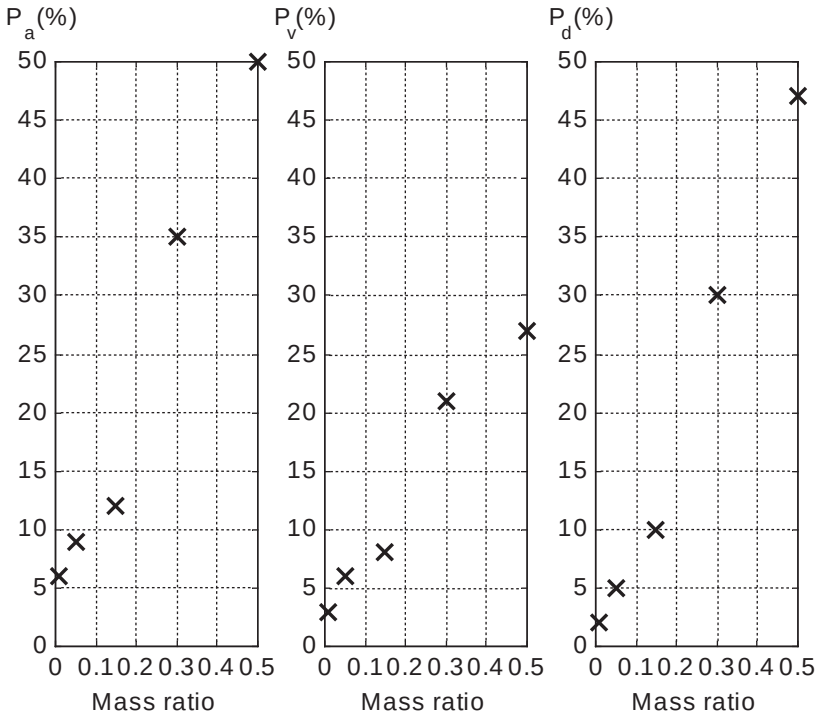

Fig. 14. Performance of the optimal semiactive-tuned mass damper compared to equivalent passive-tuned mass damper for SylmarNS earthquake.

following possible forms:

$$u = u(r_1), \quad u = u(\dot{r}_1), \quad u = u(\dot{r}_1 + \dot{z}), \quad u = u(\ddot{r}_1 + \ddot{z}). \tag{40}$$

Even though it is beyond the scope of this paper to derive new causal sub-optimal control algorithms, optimal variations of the control parameter u with time and the measurable response quantities of the main structure subject to sinusoidal input (resonance case) and the KobeEW earthquake are illustrated in Figs. 21 and 22, respectively, to investigate if it is possible to derive any closed form expression for the above given simple causal control policies.

As seen in Figs. 21 and 22, the relations between the optimal control u and the measurable response quantities of the main structure are too complex to be expressed as a closed form function even for simple harmonic excitation. So, it may be possible, but a challenging work to derive causal sub-optimal control policies that can be implemented in practice based on the generalizable information extracted from the exact optimal solutions.

7. Conclusions

The optimal seismic response behavior of a single-degree-of-freedom structure with a semiactive-tuned mass damper incorporating an MR damper has been investigated and compared

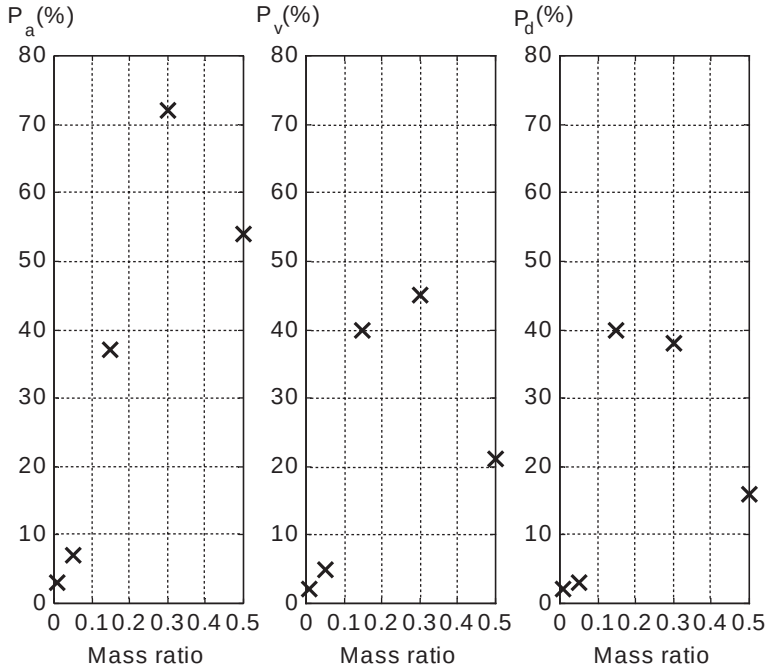

Fig. 15. Performance of the optimal semiactive-tuned mass damper compared to equivalent passive-tuned mass damper for SylmarEW earthquake.

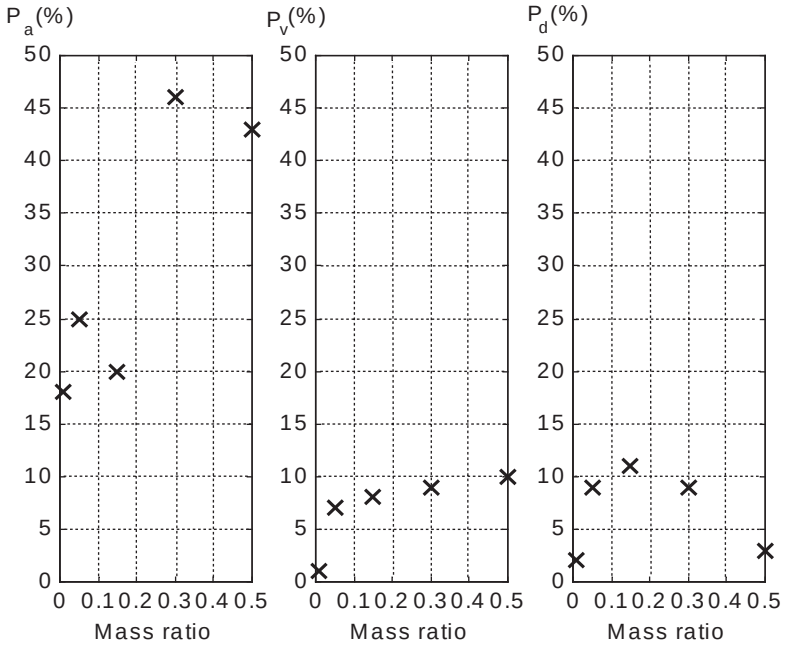

Fig. 16. Performance of the optimal semiactive-tuned mass damper compared to equivalent passive-tuned mass damper for ElcentroEW earthquake.

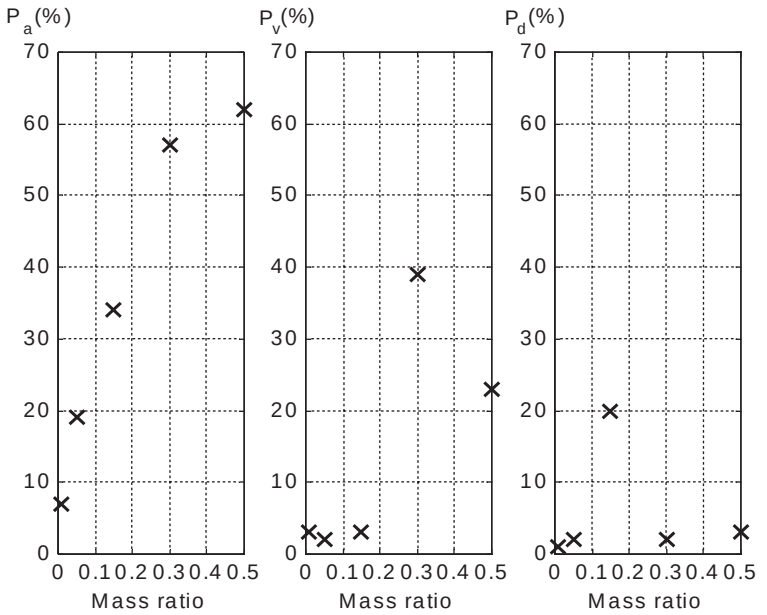

Fig. 17. Performance of the optimal semiactive-tuned mass damper compared to equivalent passive-tuned mass damper for ElcentroNS earthquake.

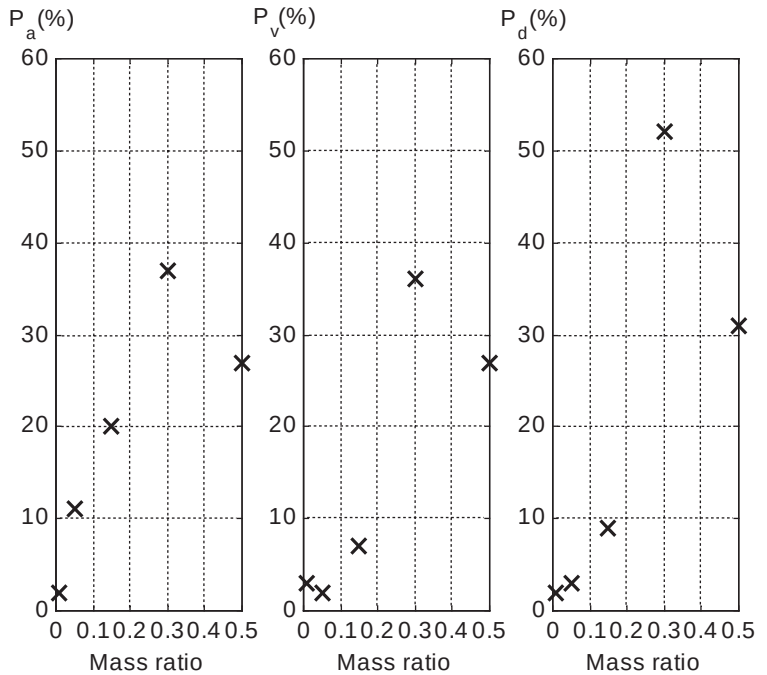

Fig. 18. Performance of the optimal semiactive-tuned mass damper compared to equivalent passive-tuned mass damper for RinaldiEW earthquake.

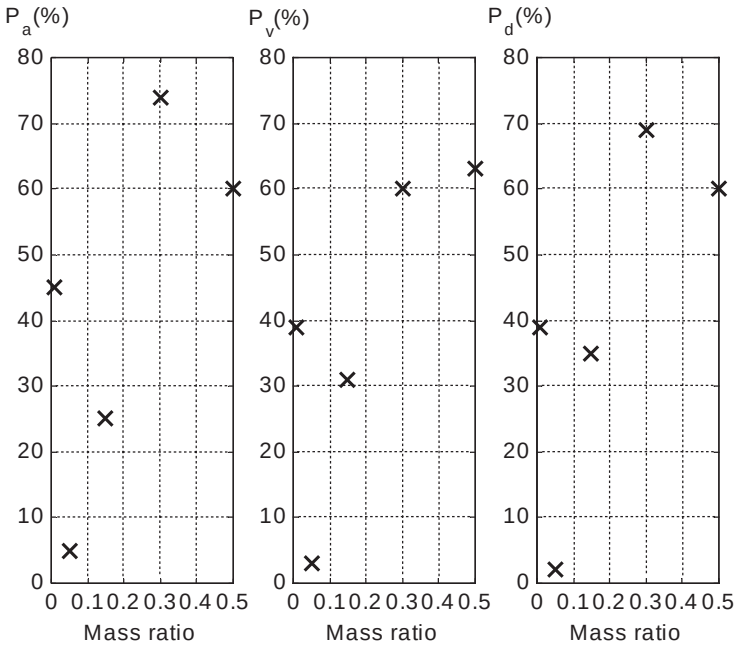

Fig. 19. Performance of the optimal semiactive-tuned mass damper compared to equivalent passive-tuned mass damper for RinaldiNS earthquake.

to an equivalent passive-tuned mass damper when the structure is excited by a broad class of excitations including sinusoidal and pulse excitations, eight real earthquakes and a simulated ground motion. Numerical solution to the two-point boundary-value problem resulting from the application of the optimal control theory is performed by using a gradient approach in which the state and costate equations are solved exactly by iterative modification of the control function. The optimal control strategy minimizes the integral of the squared absolute accelerations of the primary structure subject to the constraint that the non-linear equations of motion are satisfied.

Numerical results for the calculated acceleration, velocity and displacement performance parameters show that (a) an optimally controlled MR damper always outperforms an equivalent passive-tuned mass damper with optimized stiffness and damping parameters for all the investigated excitations, (b) the best performance for harmonic and pulse-type excitations is achieved at resonance which is very important for vibration control applications.

For the sinusoidal input: (a) The effectiveness of the semiactive-tuned mass damper with an MR damper at low frequencies ($\omega/\omega_p \approx 0.2$) is not significant, independent from the mass of the auxiliary system, compared to especially the resonance performances.

(b) The best acceleration, velocity and displacement performances are achieved at resonance in the range of $\mu = 0.05$–0.15 at the same time. This range can also be used to achieve acceptable acceleration and velocity performances at high frequencies ($\omega/\omega_p \approx 2.0$).

(c) In general, it is difficult to say that the high mass ratios result in good performance especially for acceleration although the best displacement performance at high frequencies can be obtained

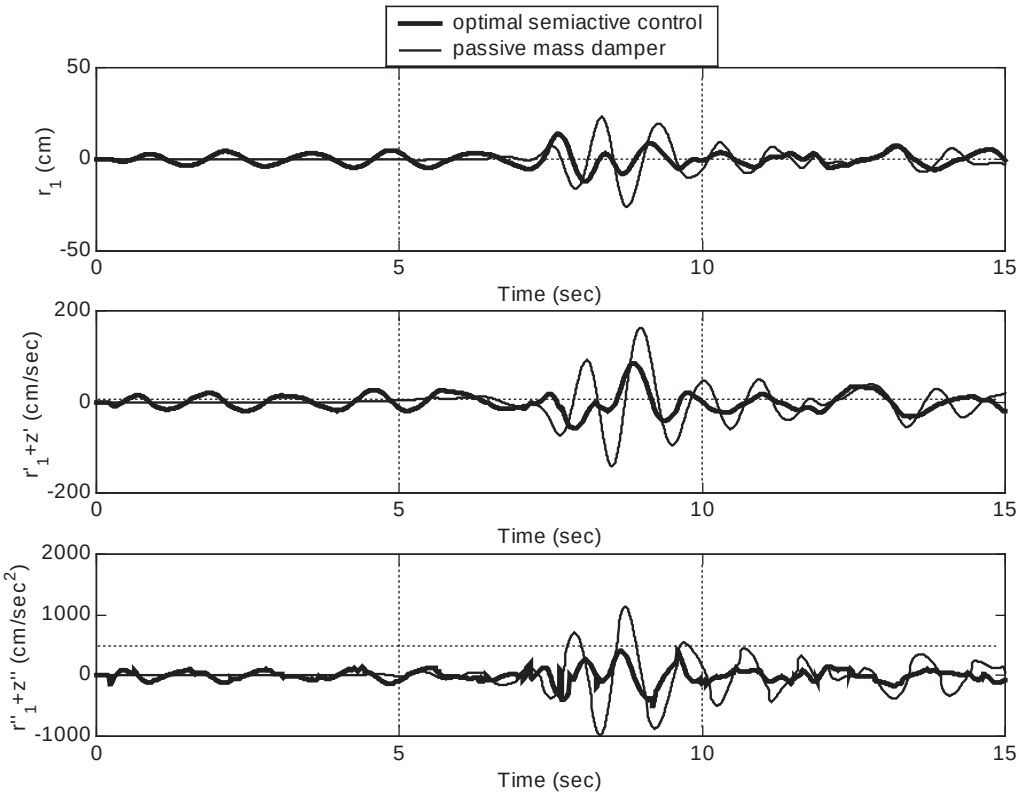

Fig. 20. Time response of the primary structure for KobeEW earthquake($\mu = 0.15$).

for $\mu = 0.30$–0.50. For the best simultaneous velocity and displacement performance at resonance, the mass ratio range can be selected as $\mu = 0.05$–0.50.

(d) For the best acceleration, velocity and displacement, simultaneous resonance performance for the harmonic excitation, the choice of the appropriate μ range is very important. A wrong choice for μ will result in a significant decrease in performance level.

For pulse-type excitations: (a) The acceleration and displacement performances in the frequency range $0.6 \leqslant (\omega_{pl}/\omega_p) \leqslant 1.4$ are much better than those at low and high frequencies for all the investigated mass ratios.

(b) The mass ratio has almost no effect on the low-frequency performances, which are low. The mass ratio $\mu = 0.50$ results in the best acceleration performance at high frequencies, while the best velocity and displacement performances are achieved for $\mu = 0.05$.

(c) The performances in the range $0.6 \leqslant (\omega_{pl}/\omega_p) \leqslant 1.4$, except for velocity performance at $(\omega_{pl}/\omega_p) = 1.4$, are not effected significantly by the change in the mass ratio. For the best resonance performance of pulse excitations, the most effective μ range can be selected as $\mu = 0.01$–0.30 for acceleration and velocity; and $\mu = 0.15$–0.50 for the displacement.

(d) It is noted that the performance percentages for all μ are very high at resonance. It indicates that the choice of the most appropriate mass ratio at resonance for pulse excitations does not seem to be as important as in harmonic case.

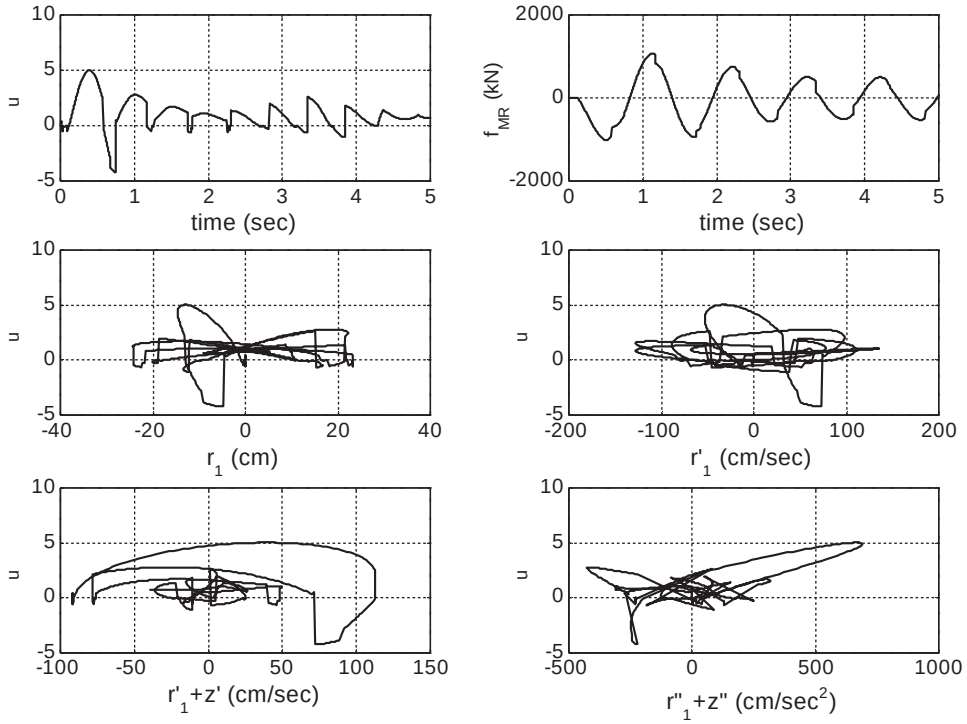

Fig. 21. Optimal semiactive MR damper force and the variation of control parameter u with time and the measurable response quantities of the main structure ($\mu = 0.05$, $\omega/\omega_p = 1$).

The optimal earthquake response of MR damper are also investigated over a wide range of recorded earthquakes including also a synthetic one because the earthquakes are naturally neither purely impulsive nor harmonic. The numerical simulation results show that it is possible to find one or more optimal mass ratios for acceleration, velocity and displacement performances of the same earthquake while in general, the optimal mass ratios are in the range $\mu = 0.15$–0.50. It is noted that the MR damper outperforms equivalent passive damper even for non-optimal mass ratios. It is also shown that the optimal response behavior of MR damper depends strongly on the random nature of earthquakes. This strong dependency indicates that the algorithms that incorporate the disturbance into causal sub-optimal control design schemes may offer additional performance. Exact optimal solutions may have some important information about how to incorporate the disturbance into control schemes. Simulation results show that it is a challenging work to get these hints from the optimal response date. However, the efforts must be underway to investigate this possibility.

While the studied optimal semiactive controller is not realizable without the a priori knowledge of the excitation, it provides a performance goal for the comparison of other proposed causal sub-optimal semiactive control policies and gives the best performance that can be achieved by the investigated semiactive device. It is concluded that the optimal MR damper implemented in a semiactive-tuned mass damper has a great potential in suppressing the structural vibrations induced by a wide range of loading conditions and this potential encourages the researches to

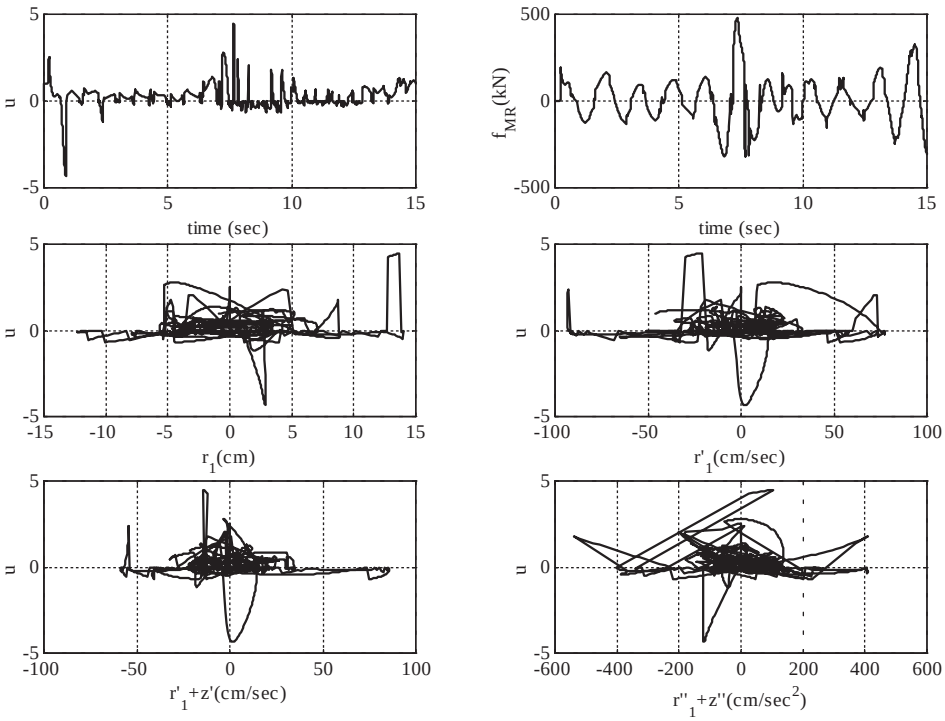

Fig. 22. Optimal semiactive MR damper force and the variation of control parameter u with time and the measurable response quantities of the main structure for KobeEW earthquake.

develop sub-optimal causal control algorithms which are capable of approaching the exact optimal performance by incorporating the disturbance into control design.

Acknowledgements

The author would like to express his appreciation to Asst. Prof. Dr. H. P. Gavin for his encouragement and advice. In addition, the reviewers' helpful comments are gratefully acknowledged.

References

[1] U. Frahm, Device for damping of bodies, US Patent No. 989, 958, 1911.
[2] J. Ormondroyd, J.P. Den Hartog, The theory of dynamic vibration absorber, Transactions of the American Society of Mechanical Engineers 50 (1928) 9–22.
[3] J.E. Brock, A note on the damped vibration absorber, Transactions of the American Society of Mechanical Engineers Journal of Applied Mechanics 13 (1946) A–284.
[4] J.P. Den Hartog, Mechanical Vibrations, 3rd Edition, McGraw-Hill, New York, 1947.
[5] E. Hahnkamm, Versammlung der Schiffbautechnische Gesellschaft, Berlin, 1935.
[6] S.H. Crandall, W.D. Mark, Random Vibration in Mechanical Systems, Academic, New York, 1963.

[7] G.B. Warburton, Optimum absorber parameters for various combinations of response and excitation parameters, Earthquake Engineering and Structural Dynamics 10 (1982) 381–401.
[8] H.C. Tsai, G.C. Lin, Optimum tuned mass dampers for minimizing steady-state response of support-excited and damped systems, Earthquake Engineering and Structural Dynamics 22 (1993) 957–973.
[9] D. Holmes, Listing of installations, Engineering Structures 17 (1995) 676–677.
[10] J. Morison, D. Karnopp, Comparison of optimized active and passive vibration absorber, Proceedings of the 14th Annual Joint Automatic Control Conference, Columbus, OH, 1973, pp. 932–938.
[11] R.A. Lund, Active damping of large structures in winds, in: H.H.E. Leipholz (Ed.), Structural Control, North-Holland, New York, 1980.
[12] J. Chang, T.T. Soong, Structural control using active tuned mass dampers, American Society of Civil Engineers Journal of Engineering Mechanics Division 106 (1980) 1081–1088.
[13] F.E. Udwadia, S. Tabaie, Pulse control of single degree of freedom system, American Society of Civil Engineers Journal of Engineering Mechanics Division 107 (1981) 997–1009.
[14] D. Hrovat, P. Barak, M. Rabins, Semi-active versus passive or active tuned mass dampers for structural control, American Society of Civil Engineers Journal of Engineering Mechanics Division 109 (1983) 691–705.
[15] M. Abe, Semi-active tuned mass dampers for seismic protection of civil structures, Earthquake Engineering and Structural Dynamics 25 (1996) 743–749.
[16] S.J. Dyke, B.F. Spencer, M.K. Sain, J.D. Carlson, Experimental verification of semi-active structural control strategies using acceleration feedback, Proceedings of the Third International Conference On Motion and Vibration Control, Vol. III, Chiba, Japan, 1996, pp. 291–296.
[17] S.J. Dyke, B.F. Spencer, M.K. Sain, J.D. Carlson, Modeling and control of magnetorhelogical dampers for seismic response reduction, Smart Materials and Structures 5 (1996) 565–575.
[18] S.J. Dyke, B.F. Spencer, M.K. Sain, J.D. Carlson, An experimental study of MR dampers for seismic protection, Smart Materials and Structures 7 (1998) 693–703.
[19] L.M. Jansen, S.J. Dyke, Semi-active control strategies for MR dampers: comparative study, American Society of Civil Engineers Journal of Engineering Mechanics 126 (8) (2000) 795–803.
[20] B.F. Spencer, S.J. Dyke, M.K. Sain, Magnetorhelogical dampers: a new approach to seismic protection of structures, Proceedings of the Conference on Decision and Control, Kobe, Japan, 1996, pp. 676–681.
[21] B.F. Spencer, S.J. Dyke, M.K. Sain, J.D. Carlson, Phenomenological model of a magnetorheological damper, American Society of Civil Engineers Journal of Engineering Mechanics 123 (3) (1997) 230–238.
[22] G.W. Housner, L.A. Bergman, T.K. Caughey, A.G. Chassiakos, R.O. Claus, S.F. Masri, R.E. Skelton, T.T. Soong, B.F. Spencer, J.T.P. Yao, Structural control: past, present and future, American Society of Civil Engineers Journal of Engineering Mechanics 123 (9) (1997) 897–958.
[23] H.P. Gavin, H. Lee, U. Aldemir, Optimal semiactive control, Proceedings of the Second European Conference on Structural Control, Paris, France, 2000.
[24] U. Aldemir, H.P. Gavin, Auto-adaptive seismic isolation, Proceedings of the ASCE Structures Congress, Washington, DC, USA, 2001.
[25] U. Aldemir, H.P. Gavin, Optimal control of earthquake response using semi-active isolation, American Society of Civil Engineers Journal of Engineering Mechanics (2001), submitted for publication.
[26] U. Aldemir, H.P. Gavin, Semi-active control of base isolated structures, American Society of Civil Engineers Journal of Engineering Mechanics (2001), submitted for publication.
[27] H.P. Gavin, U. Aldemir, Behavior and response of auto-adaptive seismic isolation, Proceedings of the Third US–Japan Cooperative Research Program in Urban Earthquake Disaster Mitigation, Seattle, WA, USA, 2001.
[28] H.P. Gavin, U. Aldemir, Optimal semiactive isolation, Proceedings of the 2001 Mechanics and Material Conference, San Diego, CA, USA, 2001.
[29] D. Karnopp, Active and semi-active vibration isolation, Transactions of the American Society of Mechanical Engineers (Special 50th Anniversary Design Issue) 117 (1995) 177–185.
[30] M. Athans, P.L. Falb, Optimal Control: An Introduction to the Theory and its Applications, McGraw-Hill Book Company, New York, 1966.

[31] U. Aldemir, M. Bakioglu, Active control based on the prediction and degree of stability, Journal of Sound and Vibration 247 (4) (2001) 561–576.
[32] M. Bakioglu, U. Aldemir, A new numerical algorithm for sub-optimal control of earthquake excited structures, International Journal For Numerical Methods in Engineering 50 (12) (2001) 2601–2616.
[33] U. Aldemir, M. Bakioglu, S.S. Akhiev, Optimal control of linear structures, Earthquake Engineering and Structural Dynamics 30 (6) (2001) 835–851.
[34] S.S. Akhiev, U. Aldemir, M. Bakioglu, Multipoint instantaneous optimal control of structures, Computers and Structures 80 (2002) 909–917.
[35] R.F. Stengel, Optimal Control and Estimation, Dower Publications Inc, New York, 1994.
[36] R.W. Clough, J. Penzien, Dynamics of Structures, McGraw-Hill Book Company, New York, 1993.
[37] H.P. Gavin, R.D. Hanson, F.E. Filisko, Electrorheological dampers, part I: analysis and design, American Society of Mechanical Engineers Journal of Applied Mechanics 63 (1996) 669–675.
[38] H.P. Gavin, R.D. Hanson, N.H. McClamroch, Electrorheological dampers, part II: testing and modeling, American Society of Mechanical Engineers Journal of Applied Mechanics 63 (1996) 676–682.
[39] H.P. Gavin, Control of seismically excited vibration using electrorheological materials and Lyapunov methods, IEEE Transactions on Control Systems Technology 9 (1) (2001) 27–36.
[40] I. Nishimura, T. Yamada, M. Sakamoto, T. Kobori, Control performance of active-passive composite tuned mass damper, Smart Materials and Structures 7 (1998) 637–653.
[41] P. Dorato, C. Abdallah, V. Cereno, Linear Quadratic Control, Prentice-Hall, New Jersey, 1995.
[42] L.S. Pontryagin, P.V. Boltianski, Mathematical Theory of Optimal Processes, Fizmatgiz, Moscov, 1962.
[43] M. Shinozuka, P. Wai, Digital simulation of short-crested sea surface elevations, Journal of Ship Research 23 (1) (1979) 76–84.
[44] Y. Ribakov, J. Gluck, Selective controlled base isolation system with magnetorheological dampers, Earthquake Engineering and Structural Dynamics 31 (2002) 1301–1324.
[45] I.H. Shames, F.A. Cozzarelli, Elastic and Inelastic Stress Analysis, Prentice-Hall, Englewood Cliffs, NJ, 1992.
[46] R. Bouc, Forced vibration of mechanical systems with hysteresis, Proceedings of the Fourth Conference on Nonlinear Oscillations, Prague, Czechoslovakia, 1967.
[47] Y.K. Wen, Method for random vibration of hysteretic systems, American Society of Civil Engineers Journal of Engineering Mechanics Division 102 (2) (1976) 249–263.
[48] B.F. Spencer, S.J. Dyke, M.K. Sain, J.D. Carlson, Phenomenological model for magnetorheological dampers, American Society of Civil Engineers Journal of Engineering Mechanics Division 123 (3) (1997) 230–238.
[49] M. Setareh, Application of semi-active tuned mass dampers to base-excited systems, Earthquake Engineering and Structural Dynamics 30 (2001) 449–462.
[50] S.B. Choi, W.K. Kim, Vibration control of a semi-active suspension featuring electrorheological fluid dampers, Journal of Sound and Vibration 234 (3) (2000) 537–546.
[51] T.T. Soong, Active Structural Control: Theory and Practice, Longman Scientific and Technical, Essex, 1990.
[52] A. Baratta, O. Corbi, On the optimality criterion in structural control, Earthquake Engineering and Structural Dynamics 29 (2000) 141–157.